Journal of Biomechanics 85 (2019) 74–83

Contents lists available at ScienceDirect

Journal of Biomechanics

journal homepage: www.elsevier.com/locate/jbiomech
www.JBiomech.com

Development of a computational fluid dynamics model for mucociliary clearance in the nasal cavity

Yidan Shang [a,b], Kiao Inthavong [b,*], Jiyuan Tu [b,c]

[a] College of Air Transportation, Shanghai University of Engineering Science, Shanghai 201620, China
[b] School of Engineering, RMIT University, PO Box 71, Bundoora, VIC 3083, Australia
[c] Key Laboratory of Ministry of Education for Advanced Reactor Engineering and Safety, Institute of Nuclear and New Energy Technology, Tsinghua University, PO Box 1021, Beijing 100086, China

ARTICLE INFO

Article history:
Accepted 4 January 2019

Keywords:
Nasal cavity
Mucus
CFD
Surface-unwrapping

ABSTRACT

Intranasal drug delivery has attracted significant attention because of the opportunity to deliver systemic drugs directly to the blood stream. However, the mucociliary clearance poses a challenge in gaining high efficacy of intranasal drug delivery because cilia continuously carry the mucus blanket towards the laryngeal region. To better understand mucus flow behaviour on the human nasal cavity wall, we present computational model development, and evaluation of mucus motion on a realistic nasal cavity model reconstructed from CT-scans. The model development involved two approaches based on the actual nasal cavity geometry namely: (i) unwrapped-surface model in 2D domain and (ii) 3D-shell model. Conservation equations of fluid motion were applied to the domains, where a mucus production source term was used to initiate the mucus motion. The analysis included mucus flow patterns, virtual saccharin tests and quantitative velocity magnitude analysis, which demonstrated that the 3D-shell model results provided better agreement with experimental data. The unwrapped-surface model also suffered from mesh-deformations during the unwrapping stage and this led to higher mucus velocity compared to experimental data. Therefore, the 3D-shell model was recommended for future mucus flow simulations. As a first step towards mucus motion modelling this study provides important information that accurately simulates a mucus velocity field on a human nasal cavity wall, for assessment of toxicology and efficacy of intranasal drug delivery.

1. Introduction

The highly vascularized nasal mucosa makes the nasal cavity a viable route for local and systemic drug delivery. In-vitro (Shah et al., 2014) and computational studies (Dong et al., 2018a, b; Ge et al., 2012; Tong et al., 2016) have investigated sprayed particle deposition distributions on nasal surfaces, which showed that the delivered drug particles had low efficacy primarily due to high deposition occurring in the anterior nasal cavity (vestibule). This region is covered with squamous epithelium that doesn't absorb the drug. To optimize nasal administration, it is necessary to understand the role nasal mucociliary clearance plays in the transport and diffusion of deposited drug particles, and this is related to the velocity field of the mucus layer on the nasal cavity surface.

For fast-action drugs, the mucociliary clearance effect helps to identify the eventual translocated position after initial deposition, relative to the therapeutic absorption time. However, for many drug formulations, the challenge is ensuring drug absorption times are faster than the clearance time. Recent by work Rygg and Longest (2016) evaluated a nasal clearance model for corticosteroid mometasone furoate. Additionally, Schipper et al. (1991) discussed strategies to increase absorption times of poorly permeating drugs that includes the class of peptides and proteins which has potential for nasal insulin therapy.

A standard method to quantify mucociliary clearance rate is the Saccharin test, where a saccharin particle is placed 1 cm behind the anterior end of the inferior-turbinate and the time is recorded until the patient perceives a sweet taste from the saccharin. The average mucociliary clearance time for a healthy adult is 7–20 min (Corbo et al., 1989; Gizurarson, 2015; Pires et al., 2009; Yergin et al., 1978), and is affected by individual nasal geometries. In a study of 249 healthy non-smokers (134 male and 115 female subjects) (Plaza Valia et al., 2008), the mean and standard deviation for

* Correspondence author.
E-mail address: kiao.inthavong@rmit.edu.au (K. Inthavong).

https://doi.org/10.1016/j.jbiomech.2019.01.015
0021-9290/

mucociliary clearance time was 17.17 min (SD of 8.43); median was 16 min (interquartile range of 12–20 min). The upper and lower limits were 6 and 36 min, respectively where only 6 subjects had a nasal mucociliary clearance time longer than 36 min.

Studies have measured the mucus velocity field using radioactive particles, which reported an average mucus velocity of 5 mm/min for a healthy adult (Illum, 2003; Mistry et al., 2009). The mucus velocity was unevenly distributed, and its variation depended on location. While, very low mucus velocity (1–2 mm/h) was observed at the vestibule region (anterior nose), higher velocities were found (8–10 mm/min) in the posterior nasal cavity (Gizurarson, 2015; Lale et al., 1998; Rusznak et al., 1994).

Since the mucus layer is an extremely thin structure (~10 μm) compared to the nasal cavity (~10 cm), it is impractical to generate a computational mesh and conduct simulations as a film-like domain attached to the 3D nasal cavity wall. Rygg and Longest (2016) proposed a method of transforming the nasal cavity wall to a 2D surface-based model and conducted CFD (Computational Fluid Dynamics) simulations on the flat domain where the flat domain transverse length was equivalent to the nasal cavity cross-sectional perimeter. Mucus was introduced uniformly into the computational domain over the surface, which transported the mucus blanket towards the nasopharynx outlet.

In this paper we applied the surface unwrapping technique proposed in Inthavong et al. (2014), which was used to map out wall shear stress, and particle deposition patterns on the intricate nasal cavity wall, onto a flat 2D-domain domain (Dong et al., 2016; Shang et al., 2017; Shang et al., 2015; Tong et al., 2016). This method extended the work by Rygg and Longest (2016) where topological features were preserved and contiguous connection between anatomical regions were retained, to account for mucus flow from the maxillary sinus into the nasal cavity. In this study, two models for CFD simulations of mucus motion were developed:

i. **unwrapped-surface model**: where the mucus velocity field was calculated from a surface mesh applied onto the 2D unwrapped nasal cavity wall;
ii. **3D-shell surface model**: where the mucus velocity field was calculated using a surface mesh attached to the 3D nasal cavity wall

Both models compared mucus velocities at different anatomical regions with experimental measurements. The comparison was aimed at answering whether the mucus uniformly introduced into the computational domain over the boundary surfaces was acceptable for predicting mucus motion.

2. Method

2.1. Mucus layer properties

The mucus is composed of two distinct layers (Fig. 1) with total thickness of 5–15 μm (Gizurarson, 2015; Mistry et al., 2009; Ugwoke et al., 2005). The upper layer is a 0.5–5 μm thick gel and consists of about 3% of an overlapping mucin network. The remainder is 90–95% water with electrolytes, serum proteins, immunoglobins, and lipids (Verdugo, 1990). Despite this composition, experimental studies showed that the mucus viscosity was as high as 10,000 times of water (Mestecky et al., 2005) due to the overlapping adhesive mucin fibres. No vertical convection occurs in the gel layer and the mucus velocity is constant along the gel layer depth.

The lower layer is the periciliary layer, which is about 7–10 μm thick (Quraishi et al., 1998). It coordinates rhythmic cilia beat that propels the gel layer towards the nasopharynx. Mucus is secreted from goblet cells and is injected into the periciliary layer before being transported into the upper gel layer. There is velocity gradient, which gradually increases in the periciliary layer from bottom to top. It is widely acknowledged that the upper gel layer constitutes the moving region of the mucociliary clearance. However, there is controversy about the transport rate of mucus in the lower periciliary layer. The traditional hypotonic-defensin hypothesis and ciliary stroke analysis consider the periciliary layer to be stationary when compared to the upper gel layer (Blake and Sleigh, 1974; Fulford and Blake, 1986; King et al., 1993; Satir and Sleigh, 1990; Sleigh, 1977), whereas alternative hypothesis state the transport rate of periciliary fluid is similar to the transport rate of mucus in the upper gel layer (Matsui et al., 1998). As a proof-of-concept work, the upper gel layer was only considered and the mucus density was set to $1,000 kg \cdot m^{-3}$. The optimal value for mucus viscosity was $12 Pa \cdot s$ suggested by Puchelle et al. (1987)'s experimental study.

2.2. Nasal cavity division based on mucus producing regions

An anatomical nasal cavity model was reconstructed from CT-scan data of a 48-year old healthy Asian male, used in previous papers (Dong et al., 2018b; Shang et al., 2018; Shang et al., 2015). Fig. 2(a, i) shows the 3D model viewed from the right-chamber-side, and from the top.

The model was divided into anatomical regions based on major mucus producing regions. At the entrance of the nose is the vestibule region, which is non-ciliated (Marttin et al., 1998), and this extends to approximately the anterior third of the nasal cavity

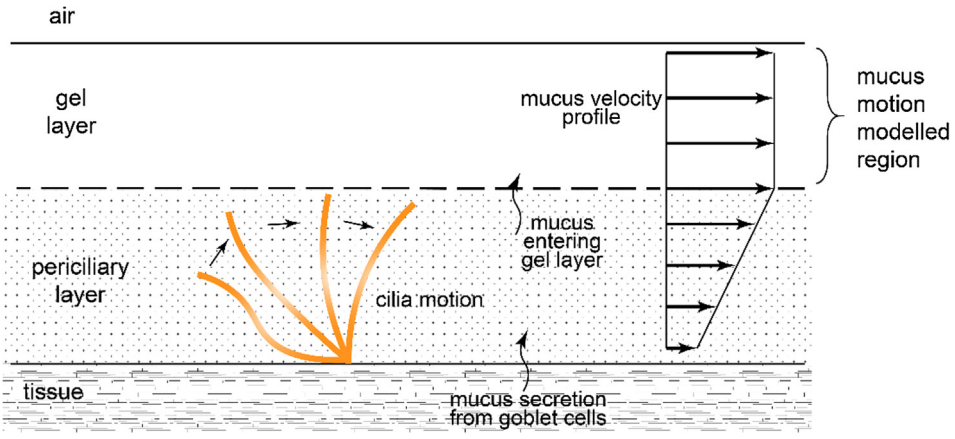

Fig. 1. Nasal mucus composed of two distinct layers with total thickness 5–15 μm (i) upper gel layer consisting of overlapping mucin fibrous network, and (ii) lower periciliary layer consists of cilia.

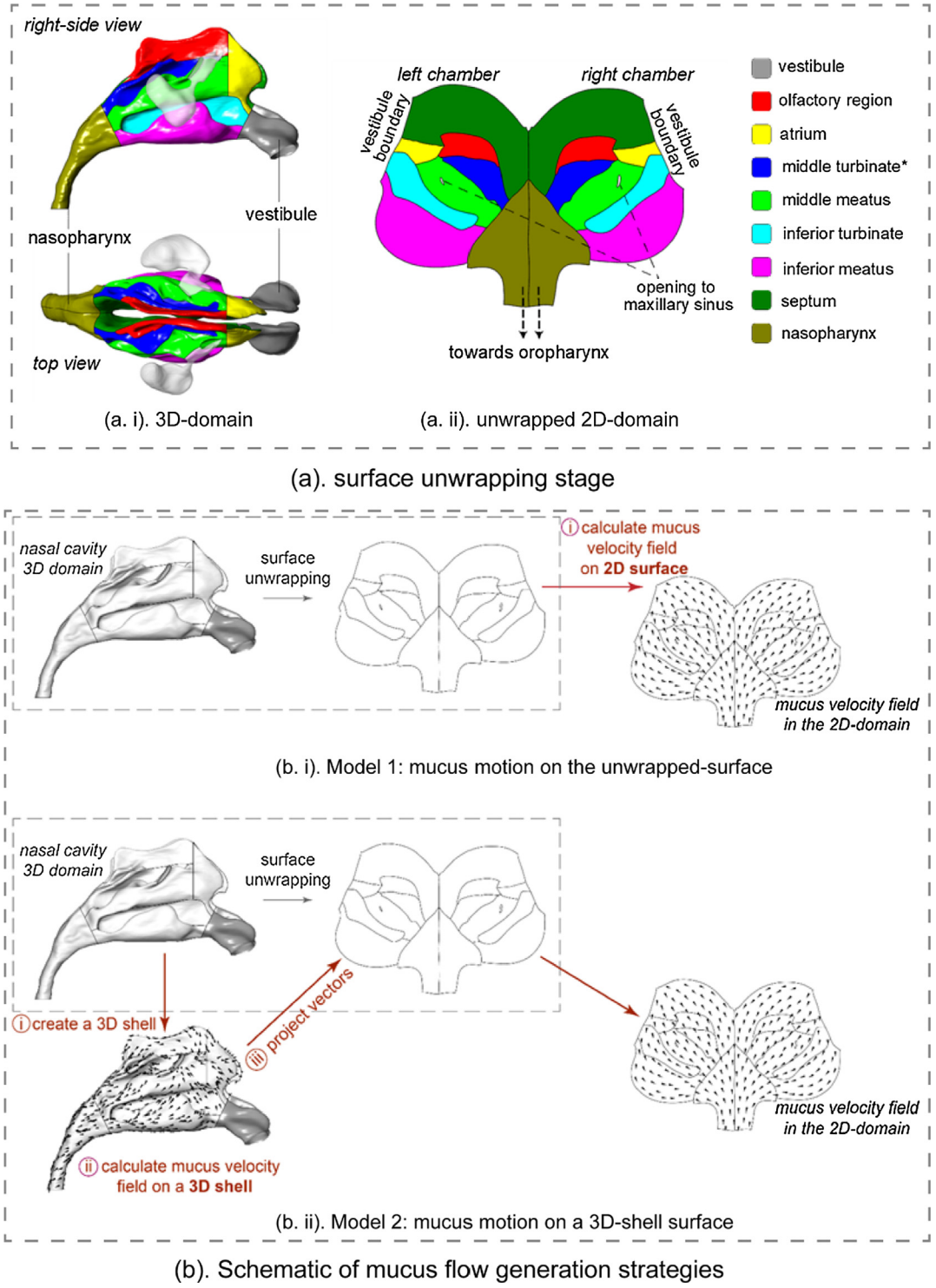

Fig. 2. The nasal surface division strategy and surface-wrapping technique used for mucus motion simulation. (a) Nasal cavity divided into multiple regions. The vestibule (grey), and the nasopharynx represent the anterior and posterior regions, respectively. In the middle is the main nasal passage which was divided into seven further sub-regions: vestibule, atrium, middle turbinate, middle meatus, inferior turbinate, inferior meatus, and septum. (b) Schematic of Model 1 (b. i., unwrapped-surface model) where the mucus velocity is calculated directly from the 2D unwrapped surface, and Model 2 (b. ii., 3D-shell model) where a shell around the 3D model is first created, and the mucus velocity is calculated directly from the 3D shell domain, and projected to the 2D unwrapped surface. *The middle turbinate region also included superior meatus.

(Mygind and Dahl, 1998). Following this is the respiratory epithelium, which is the major lining of the human nasal cavity that involves mucociliary clearance. The respiratory epithelium contains both non-ciliated, and ciliated columnar cells, goblet cells, and basal cells. Cilia starts occurring just behind the front edge of the inferior turbinate, and ciliated cell density generally increased in the antero-posterior direction, while there were few regions of non-ciliated epithelial cells (Halama et al., 1990). Thus, the cell distribution in the nasal cavity is non-uniform.

Mucus is secreted by goblet cells in the respiratory epithelium (Gelman and Meyer, 1979; Quraishi et al., 1998). It is also secreted within the maxillary sinuses which flow from inside the sinus and

onto the nasal cavity surface via the maxillary ostium (Ballenger and Snow, 2003; Lale et al., 1998; Rusznak et al., 1994). There is a large production of mucus in the maxillary sinus due to the highest density of ciliated cells near the maxillary ostium (Halama et al., 1990).

The left and right vestibule regions (labelled in the Fig. 2(a, i)) were separated in the nasal geometry, since they were non-ciliated regions. The frontal sinuses, ethmoid sinuses and sphenoid sinuses were omitted due to limited CT-scanned data resolution. The maxillary sinuses were retained for volume and surface area calculations. In the middle is the main nasal passage, which was divided into seven sub-regions. Table 1 provides the surface area and volume of the main passage and maxillary sinus of the left, and right chambers of the nasal cavity.

A surface-unwrapping technique transformed the 3D surface boundary onto a flat 2D domain (Fig. 2(a, ii)). The left and right chambers were separated by the nasopharynx, and the posterior septum wall boundaries. The vestibule was omitted during this step since it neither secretes mucus nor hosts cilia, and the 2D domain is labelled with the vestibule boundary in its place. Although a small portion of mucus enters the vestibule and exits the nostrils, it can be ignored when compared to the amount of mucus produced per day in the nasal cavity of 1–2 L (Baroody, 2007). Additionally, Rusznak et al. (1994) measured mucus velocity in the anterior nose (vestibule), which was 1–2 mm/h. This is negligibly slow compared to an average velocity of 5 mm/min for the whole nasal cavity and velocity of 8–10 mm/min at the posterior nose. The maxillary sinus geometry was also omitted during the unwrapping process, due to its complex geometry. However, the maxillary ostia were retained to form a boundary allowing a mucus production source term.

2.3. Mucus motion model development

We propose two models to reproduce moving mucus and its velocity distribution, Model 1: Mucus motion on the **unwrapped-surface** and Model 2: Mucus motion on a **3D-shell surface** shown schematically in Fig. 2b. In Model 1 the mucus velocity was calculated on the unwrapped-surface domain using conservation equations. In Model 2 the mucus velocity was calculated on an outer single-layer shell covering the 3D nasal cavity, using conservation equations. To allow direct comparison of the mucus velocity field, data from the 3D-shell model was projected to its equivalent 2D unwrapped surface. The steady-state continuity equation with a source term was used,

$$\rho\left(\nabla \cdot \vec{\boldsymbol{v}}\right) = \dot{f}_{source} \tag{1}$$

where ρ is density of mucus, $\dot{f}_{source}$ is mucus mass generation in the computational domain and $\vec{v}$ is the mucus velocity. The steady-state momentum equation used was,

$$\rho\left(\vec{\boldsymbol{v}} \cdot \nabla\right)\vec{\boldsymbol{v}} = -\nabla p + \mu\nabla^2\vec{\boldsymbol{v}} \tag{2}$$

where p is the pressure and μ is the mucus viscosity.

2.4. Mesh generation and CFD setup

In each model, a surface mesh with triangular elements was created in Ansys ICEM 18.2, and then extruded one cell height to represent a thickness of 10 μm. The minimum mesh skewness measured in ICEM were 0.25 for the 3D-shell model and 0.42 for the surface-unwrapped model. A mesh independence test was performed by calculating the average mucus velocity in the inferior meatus, which became stable when the global mesh element size reached 0.6 mm. To guarantee the accuracy, the mesh element size was set to 0.5 mm in this study.

To represent realistic mucus production into the computational domain, a uniform mass source term ($\dot{f}_{source}$) was applied (Fig. 3). The mass source term was proportional to the nasal cavity surface area, and the representative mucus layer height, h, set to 10 μm.

$$\dot{m}_{nasal} = \dot{f}_{source} * A_{nasal_surface} * h \tag{3}$$

Ballenger and Snow (2003) showed a mucus blanket covered the entire maxillary sinus surface area and that it flowed towards the maxillary ostium. At the ostium boundary, the mucus mass flow rate was assumed to be proportional to its maxillary sinus surface area, and proportional to the mucus flow of the nasal cavity surface area, defined as:

$$\dot{m}_{ostium} = \dot{f}_{source} * A_{sinus} * h \tag{4}$$

This means the mucus velocity was derived purely by mass conservation constrained by a constant mucus height and driven by a mass source (mucus generation) which is the $\dot{f}_{source}$ term. No shear stress occurred between nasal wall and mucus, but shear stress does exist inside the flow due to the viscous term in the momentum equation (Eq. (2)).

The mucus accumulated in the single-layer computational domain, and due to mass conservation, moved towards the nasopharynx outlet. Although in principle the upper mucus (gel) layer is transported by cilia motion, the model relies on the momentum equation to redistribute the mucus flow velocity field similar to (Rygg and Longest, 2016) and (Rygg et al., 2016)'s studies. For each model, the mucus production rate (source term) was determined in such way that the average mucus velocity over the nasal cavity wall reached 5 mm/min (Illum, 2003; Mistry et al., 2009; Pires et al., 2009; Ugwoke et al., 2005). As mucus flow patterns vary between the models, the exact mucus production rates don't have to be the same. The final mucus production rates were $\dot{f}_{source} = 0.9224 kg \cdot s^{-1} \cdot m^{-3}$ for the 3D-shell model and $\dot{f}_{source} = 0.8030 kg \cdot s^{-1} \cdot m^{-3}$ for the surface-unwrapped model.

Given the high viscosity and the low velocity magnitude, the Reynold's number $Re = \rho UD/\mu$ was below 1e-4 and the mucus flow was classified as creeping laminar flow. The discretization schemes were second-order, and the SIMPLE coupling was used. Convergence was set by residuals reaching 1e-6 and the simulations were performed using Ansys-Fluent v18.2. The boundary condition at the nasopharynx exit was set as outflow, and the remaining surfaces were treated as slip wall boundaries, thus no shear effects at the wall.

Table 1
Surface area and volume of major components of the nasal cavity.

Regions	Vestibule	Main passage*		Nasopharynx	Maxillary sinus	
		Left	Right		Left	Right
Area (mm^2)	1627.6	8632.7	8458.3	1641.9	1572.2	1131.8
Volume (mm^3)	3317.8	7178.6	11227.5	4682.6	3505.9	2012.3

* volume of main passages calculated for region between the vestibule and nasopharynx regions.

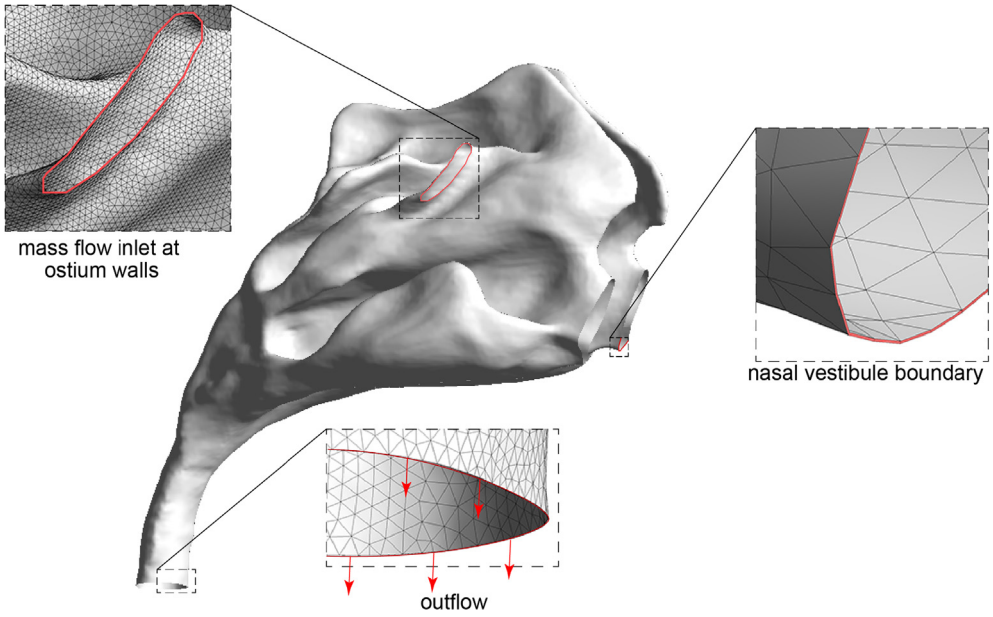

Fig. 3. Computational mesh for unwrapped-surface model and 3D-shell model.

3. Results

3.1. Mucus velocity fields

Mucus velocity fields for the unwrapped-surface and 3D-shell models (Fig. 4b) were indicated by unit vectors and velocity magnitude indicated by the colour band. General velocity flow behaviour was similar in both models, where there is a symmetric pattern between the left and right chambers. Mucus accelerated from the anterior to posterior nasal cavity with velocities at the nasopharynx.

In the unwrapped-surface model (Fig. 4(b. i)) the contour plot showed a smooth change in velocities from the vestibule boundary steadily increasing to a peak velocity at the nasopharynx. The low velocity regions were concentrated near the vestibule boundary. In the 3D-shell model (Fig. 4(b, ii)) low velocity regions were found across all anatomical regions in the main nasal passage except for the septum and nasopharynx. A velocity jump was found near the choana, where the mucus velocity rapidly increased from ~10 mm/min to >30 mm/min. Another noticeable high velocity region was found at the inferior septum boundary, which was the floor of the nasal cavity wall.

Mucus motion differed between the two models. For the unwrapped-surface model, the mucus motion followed the geometry from the vestibule boundary towards the nasopharynx, while for the 3D-shell model there was a radial pattern originating from the maxillary ostium

3.2. Virtual saccharin test

In clinical applications, a standard method called the saccharin test is frequently used to check the condition of the mucociliary clearance. A saccharin particle is placed 1 cm behind the anteroinferior turbinate and the elapsed time is recorded until a patient can detect the taste of saccharin. It takes 7–20 min for a healthy adult to perceive the saccharin (Gizurarson, 2015). We conducted a 'virtual saccharin test' by introducing a particle at the anterioinferior turbinate and calculated its elapsed time as it moved along the mucus velocity field until the nasopharynx exit.

To avoid variations caused by the different locations, the 'virtual saccharin' test was performed from three locations A, B and C, which were 0.6 cm, 1.0 cm and 1.4 cm behind the anterior inferior turbinate. The particle trajectories on the unwrapped-surface model and the 3D-shell model are shown in Fig. 4c, where the particles travelled along the lateral sides of the nasal cavity wall and moved through the inferior meatus before entering the nasopharynx. The paths were coloured by residence times and Table 2 summarises the clearance times (time taken to travel to nasopharynx) where similar times were achieved between left and right chambers of both models. However, for the unwrapped-surface model the clearance times ranged between 34.9–68.3 min, while for the 3D-shell model it was 14.8–27.2 min; a difference of 2.5×. In the unwrapped-surface model, the clearance time decreased when the saccharin release point was posteriorly located, while for the 3D-shell model the opposite occurred.

3.3. Mucus velocity on a characteristic line

Investigations of mucus motion measured the mucus velocity distribution from anterior to posterior middle turbinate (Gizurarson, 2015; Rusznak et al., 1994). For comparison, the mucus velocity magnitude along a characteristic line (Fig. 5a) starting at the anterior inferior turbinate and ending at the nasopharynx was plotted for both models (Fig. 5b). Although the line coordinate is defined from the unwrapped geometry, the velocity magnitude values were obtained by transforming the velocities from the 2D geometry domain to the 3D geometry domain to allow direct comparisons with experimental measurements (Gizurarson, 2015; Rusznak et al., 1994).

Fig. 5b shows the mucus velocity increasing as it moved towards the nasopharynx. For the unwrapped-surface model, the velocity increased smoothly from nearly 0 mm/min at the nasal valve to 7 mm/min at the posterior inferior turbinate. The velocity remained relatively constant in the posterior middle meatus before increasing to 16 mm/min at the nasopharynx. For the 3D-shell model, the velocity decreased from 3 mm/min to ~1 mm/min and then increased to 3 mm/min in the inferior turbinate region. In the posterior middle meatus, the velocity increased rapidly from

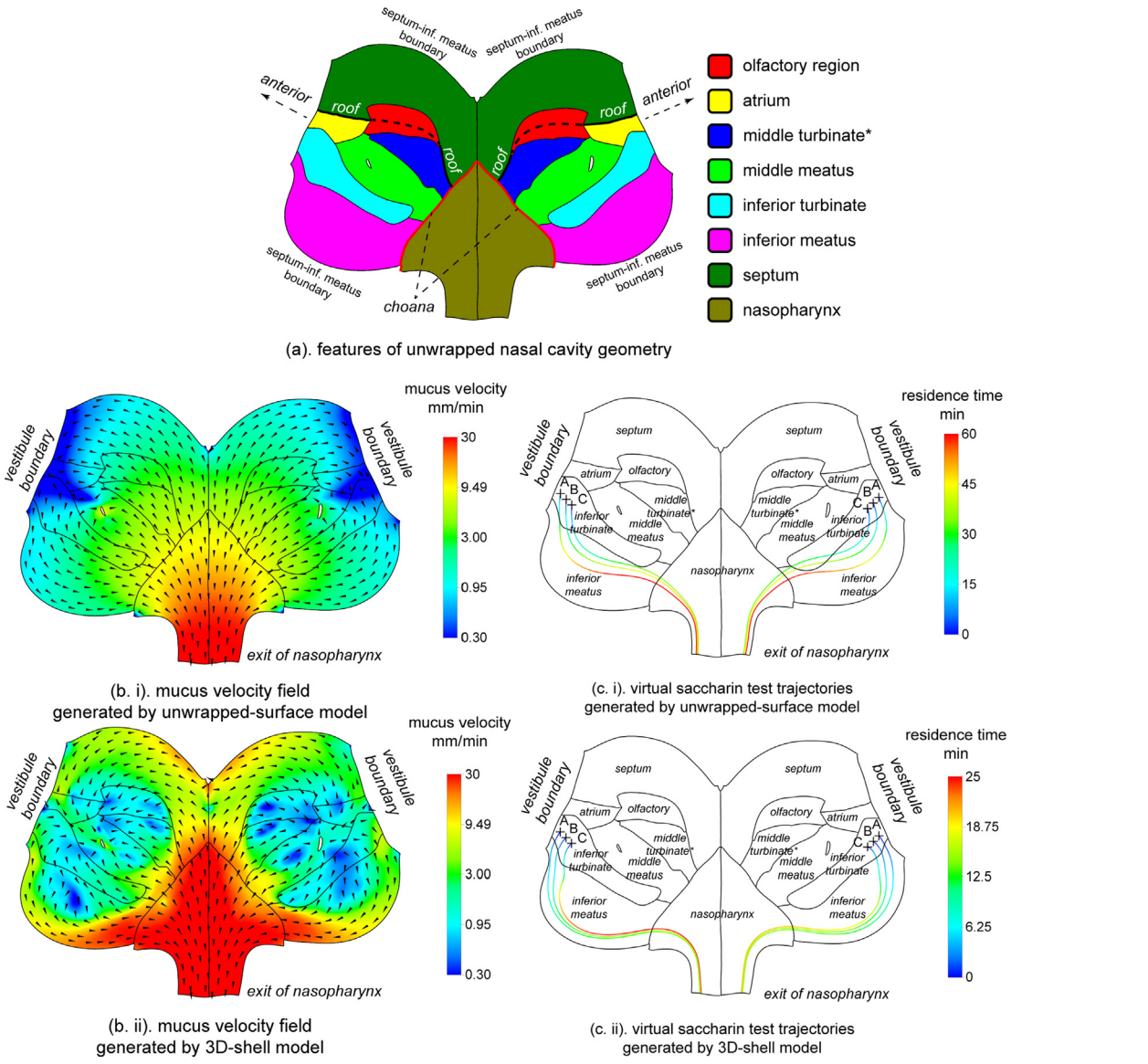

Fig. 4. Mucus flow fields generated from unwrapped-surface model and 3D-shell model are visualised in 2D view. (a) Some extra features of unwrapped nasal cavity are shown for flow fields comparisons. (b) Mucus velocity directions are visualised with the background of velocity magnitude. for (a. i) unwrapped-surface model and (a. ii). 3D-shell model. (c) Virtual saccharin test on mucus velocity field generated by (c. i). unwrapped-surface model and (c. ii). 3D-shell model.

Table 2
Clearance times of 'virtual saccharin particles' placed in locations A, B and C in left and right nasal chambers.

Nasal chamber	Model	Clearance time (min)			
		Location A	location B	Location C	Average
Left side	Unwrapped-surface	68.3	49.3	37.9	51.8
	3D-shell	14.8	17.2	27.2	19.7
Right side	Unwrapped-surface	62.6	45.9	34.9	47.8
	3D-shell	15.4	17	21.4	17.9

3 mm/min to 11 mm/min, and continued to increase to 38 mm/min at the nasopharynx.

3.4. Mucus velocity on a cross-section

Fig. 6a shows a vertical cross-section created 6 cm inside the nasal passage to examine mucus velocity distribution along the cross-section perimeter. The perimeter was projected onto the 2D domain of the unwrapped geometry where the starting and end points were the same location that connected the cross-section together. The origin of the perimeter (starting point) was taken at the interface of the inferior meatus and septum. The distance from the origin follows the depicted arrows in Fig. 6a. The velocity magnitude along the perimeter between the two models are shown for the left (Fig. 6b) and right chambers (Fig. 6c).

Both models produced similar velocity profiles between the left and right nasal chambers. However, between the two models, the velocity profiles were very different. The unwrapped-surface

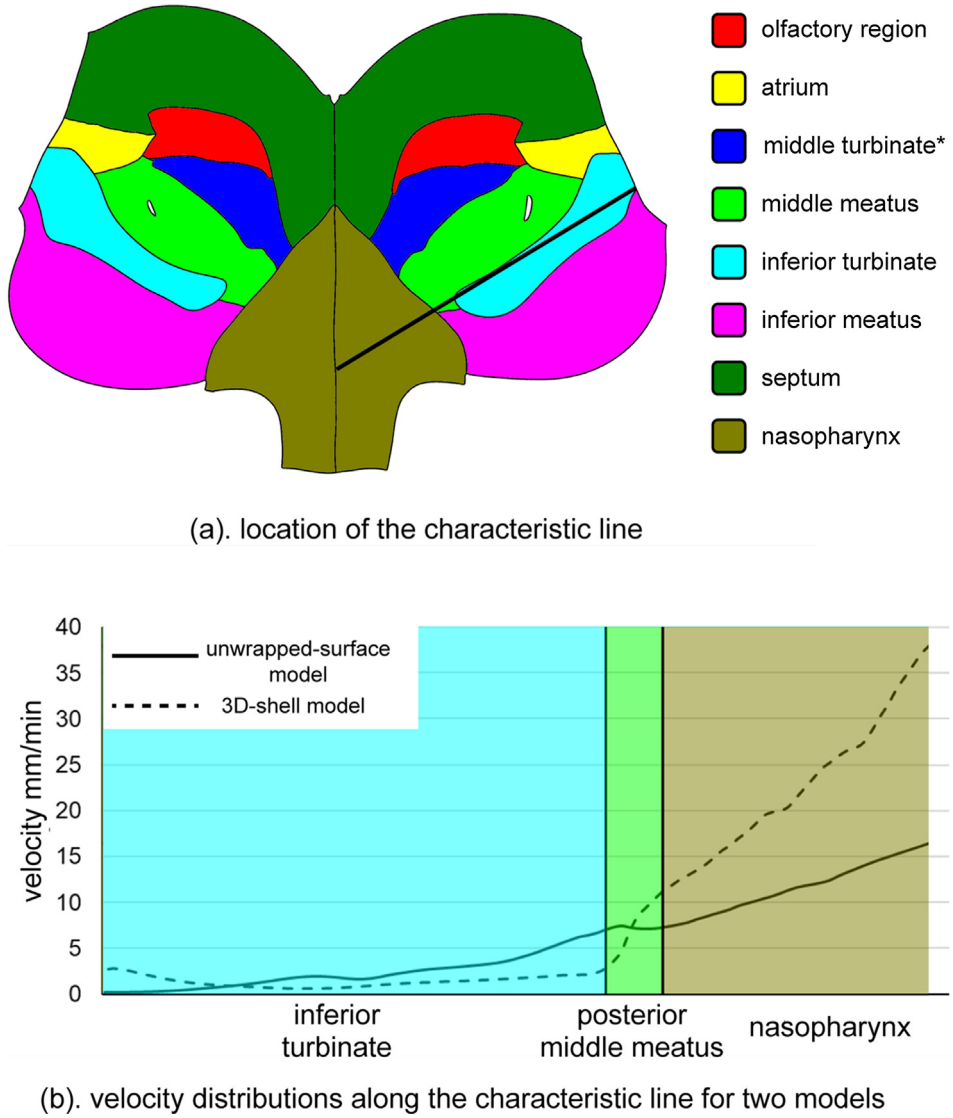

Fig. 5. Mucus velocity distributions on a characteristic line based on two models.

model presented relatively similar velocity along the perimeter, with higher velocities reaching 7 mm/min at middle meatus and middle turbinate, and lower velocities around 1 mm/min at the inferior meatus, inferior turbinate, olfactory and septum. For the 3D-shell model, higher velocities were concentrated at the inferior meatus and septum, reaching up to 10.5 mm/min at the interface between them. At other regions, the mucus velocity was much lower fluctuating between 1 and 3 mm/min.

4. Discussion

We present computational models for detailed mucus velocity distribution on the nasal cavity wall. This is a first study to visualise the mucus velocity distributions on the anatomical nasal regions. In experimental studies, radioactive particles ^{88m}Tc and ^{111}I are often used to measure local mucus velocity (Lale et al., 1998). However, the analysis is hindered by highly overlapping nasal structures, which obstruct the γ-camera to accurately detect the location of the radioactive particles leading to approximate mucus flow patterns.

Negligible mucus velocity (~1–2 mm/h) detected in the anterior part of nose (Rusznak et al., 1994) confirmed the rationale for removing the vestibule from the models. The reported velocity in the posterior nose was 8–10 mm/min (Rusznak et al., 1994), which was slighter larger than the predicted velocity of 7.0–7.3 mm/min from the unwrapped-surface model and matche the simulated velocity 2.7–11.6 mm/min from the 3D-shell model. Quinlan et al. (1969)'s study described particle movement on the medial surface of the inferior turbinate moving laterally to the inferior meatus and then posteriorly towards the choana. Velocity fields from both unwrapped-surface and 3D-shell models showed good agreement with this description. Andersen et al. (1971)' study observed an area in the anterior nasal cavity where the mucus moved forward. This validates the 3D-shell model as forward-moving mucus was found in the anterior region of the maxillary ostium, while the unwrapped-surface model did not. Andersen et al. (1971) also observed abnormal spots in the middle passage where the mucus velocity was extremely slow. This phenomenon matched the low velocity distribution generated by 3D-shell model very well, whereas no such low velocity region was found in the unwrapped-surface model.

The saccharin test is significantly affected by individual variation and was reported as taking 7–20 min for healthy adults (Corbo et al., 1989; Gizurarson, 2015; Pires et al., 2009; Yergin

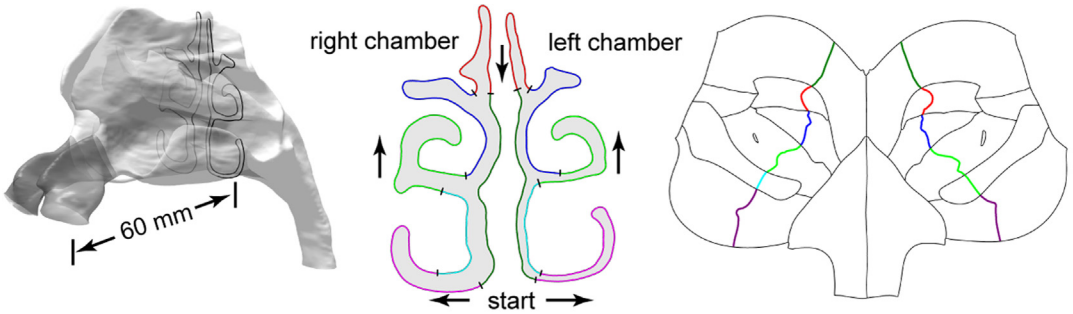

(a). location of the cross-section and its projection in the unwrapped geometry

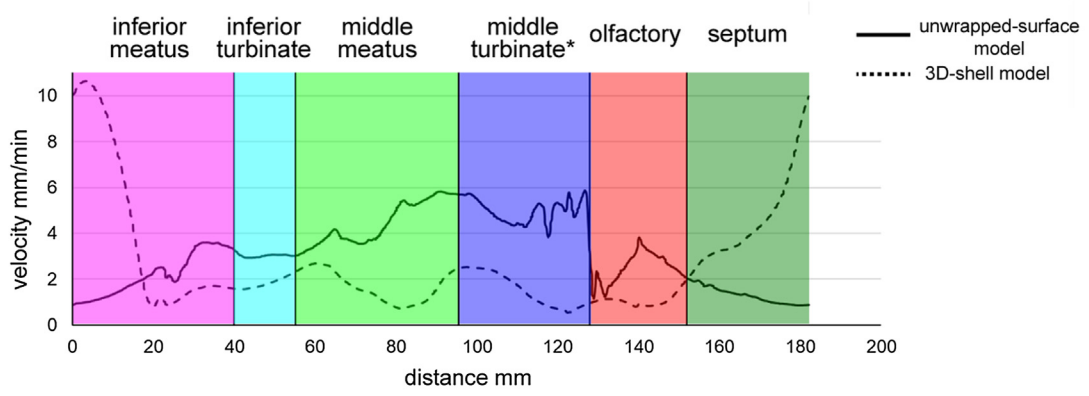

(b). velocity distributions on left chamber

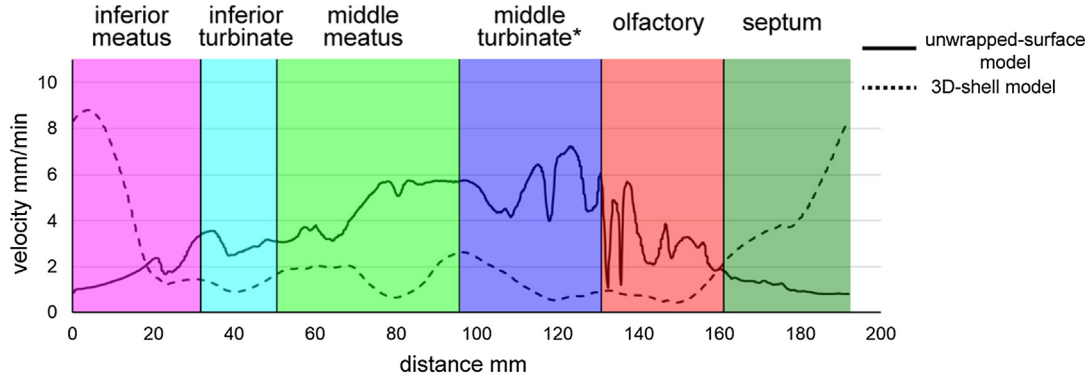

(c). velocity distributions on right chamber

Fig. 6. Cross-sectional velocity distributions for unwrapped-surface model and 3D-shell model. The cross-section is 60 mm behind the centre of nostrils. *The middle turbinate region also included superior meatus.

et al., 1978) and should not exceed 36 mins when taking high individual variations into account (Plaza Valia et al., 2008). The 'virtual saccharin' test time of 34.9–68.3 min predicted by the unwrapped-surface model exceeds the range, even when accounting for individual anatomical variations. The 3D-shell model produced much better agreement with clearance times ranging between 14.8–27.2 min. The mucus velocity field generated by the 3D-shell model exhibited a more efficient pattern for mucociliary clearance than in the unwrapped-surface model. The virtual saccharin particles immediately travelled along the floor of the nasal cavity wall after release and joined a region of high mucus velocity flow.

There were large differences in the mucus velocities between unwrapped-surface and 3D-shell models. For each model, the mucus velocity field was generated by the continuity equation

Table 3
Regional surface area in 3D and unwrapped domains.

Name of regions	Area mm^2		Area Ratio
	3D domain	Unwrapped domain	
Olfactory	1890.2	959.3	0.51
Atrium	664.4	545.6	0.82
Middle turbinate+	1951.8	1169.9	0.60
Middle meatus	3306.5	2068.8	0.63
Inferior turbinate	1763.0	1689.8	0.96
Inferior meatus	3318.2	3755.7	1.13
Septum	4111.6	5150.3	1.25
Nasopharynx	1642.0	3326.0	2.03
Total	18647.7	18665.4	1.00

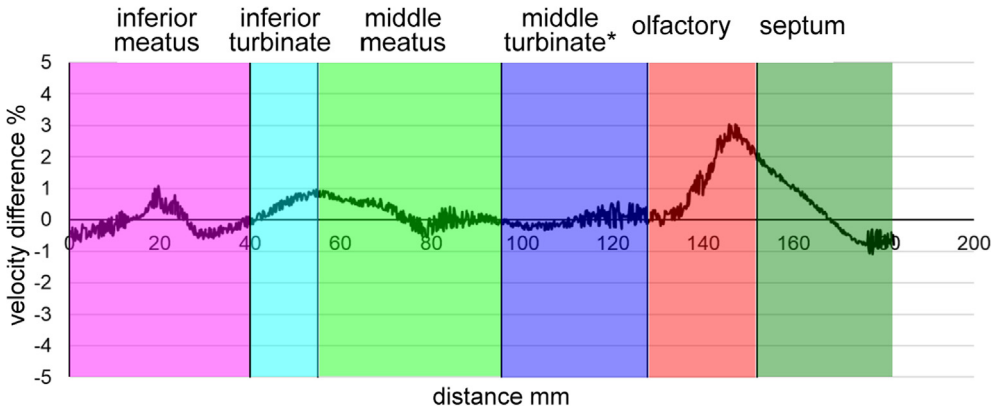

(a). velocity difference on left chamber

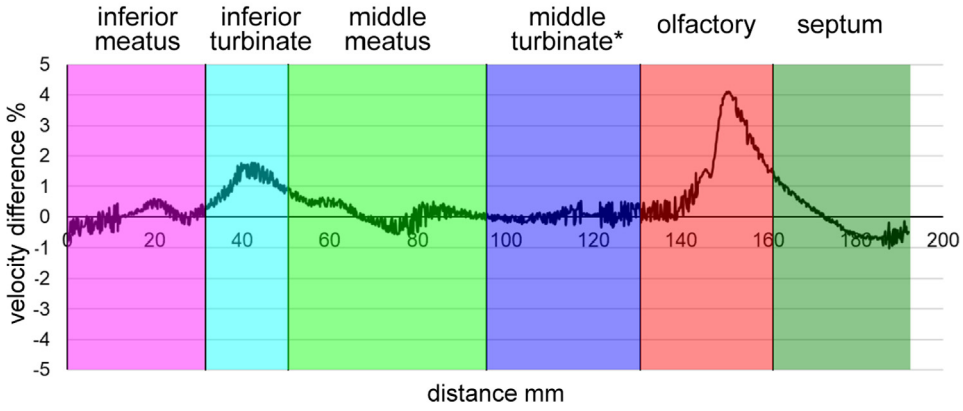

(b). velocity difference on right chamber

Fig. 7. Cross-sectional velocity difference between modelling with and without gravity effects (upright position). The cross-section was taken at 60 mm behind the nostrils. The velocity difference was defined as $(v_{gravity} - v_{no-gravity})/v_{no-gravity} * 100\%$. *The middle turbinate region also included superior meatus.

with a uniform source term and constrained by the nasal cavity surface. Due to the unwrapping process from 3D domain to the 2D domain, the surface mesh was significantly deformed. Comparisons of regional surface areas between unwrapped-surface and 3D-shell models are listed in Table 3. The area ratio was defined as the ratio of regional area in the 3D domain and its corresponding area in the 2D domain. The largest and smallest ratios were found at the nasopharynx and olfactory regions, respectively. As a result, a lower averaged velocity at the nasopharynx and a higher average velocity at the olfactory region were found for the unwrapped-surface model, compared to the 3D-shell model. Therefore, we recommend avoiding simulations of mucus flow on an unwrapped nasal domain. Instead, the 3D-shell model is more suitable to predict the mucus velocity field on the nasal cavity wall.

For simplicity, the mucus velocity field was calculated without gravity. To estimate its effect, the gravity acceleration $9.8 m/s^2$ was applied to the -*y* direction of the 3D-shell model (replicating upright standing position), and the velocity distribution at a cross-section was compared to that in the original 3D-shell model. The location of the cross-section was identical to that in Fig. 6 and the velocity difference was defined as $(v_{gravity} - v_{3d-shell})/v_{3d-shell} * 100\%$. Fig. 7 showed that the mucus velocity change caused by gravity was less than 5% for both chambers, and the peak difference occurred at olfactory regions, with 3.0% for the left chamber and 4.2% for the right chamber. The gravity has minimal effects on the mucus velocity field, and is reasonable to be ignored for the majority of mucus motion simulations.

5. Conclusion

Mucociliary clearance is critical to the efficacy of intranasal drug delivery. Mucus motion on the human nasal cavity wall was simulated using CFD by two approaches, namely unwrapped-surface model and 3D-shell model. Validation of the models compared overall mucus velocity patterns, virtual saccharin particle tracking and quantitative mucus velocity magnitude distributions with existing experimental data. Based on the study, the following conclusions were drawn:

- Mucus was introduced as a mass source term to initiate mucus flow within the nasal cavity, where the 3D-shell model exhibited higher velocities, particularly near the choana.
- In the main passage region, the 3D-shell model resulted in a radial velocity pattern originating from the maxillary ostium whereas the unwrapped-surface model presented a mucus velocity field with a uniform direction.
- The velocity magnitude distributions on a cross-sectional perimeter illustrated the mucus was concentrated along the floor of the nasal cavity in the 3D-shell model whereas in the unwrapped-surface model, relatively higher velocity was found in the middle meatus and middle turbinate.
- The virtual saccharin test showed that saccharin clearance time in the 3D-shell model had better agreement with experimental data acquired from healthy adults.

Of the two models, the 3D-shell model produced much better and more realistic results that matched existing experimental data compared with the unwrapped-surface model. This lays a solid foundation for future predictions on drug absorption via intranasal drug delivery using the 3D-shell model.

Acknowledgements

This study was funded by the National Natural Science Foundation of China (Grant No. 81800096) and Australian Research Council (Project ID: DP160101953).

Conflict of Interest

The author declares no conflict of interest.

References

Andersen, I., Lundqvist, G.R., Proctor, D.F., 1971. Human nasal mucosal. Arch. Environm. Health: Int. J. 23, 408–420.
Ballenger, J.J., Snow, J.B., 2003. Ballenger's otorhinolaryngology: head and neck surgery. Pmph-usa.
Baroody, F.M., 2007. Nasal and paranasal sinus anatomy and physiology. Clin. Allergy Immunol. 19, 1.
Blake, J.R., Sleigh, M.A., 1974. Mechanics of ciliary locomotion. Biol. Rev. 49, 85–125.
Corbo, G., Foresi, A., Bonfitto, P., Mugnano, A., Agabiti, N., Cole, P., 1989. Measurement of nasal mucociliary clearance. Arch. Dis. Child. 64, 546–550.
Dong, J., Shang, Y., Inthavong, K., Chan, H.-K., Tu, J., 2018a. Numerical comparison of nasal aerosol administration systems for efficient nose-to-brain drug delivery. Pharm. Res. 35, 5.
Dong, J., Shang, Y., Inthavong, K., Chan, H.-K., Tu, J., 2018b. Partitioning of dispersed nanoparticles in a realistic nasal passage for targeted drug delivery. Int. J. Pharm. 543, 83–95.
Dong, J.L., Shang, Y.D., Inthavong, K., Tu, J.Y., Chen, R., Bai, R., Wang, D.L., Chen, C.Y., 2016. Comparative numerical modeling of inhaled nanoparticle deposition in human and rat nasal cavities. Toxicol. Sci. 152, 284–296.
Fulford, G.R., Blake, J.R., 1986. Muco-ciliary transport in the lung. J. Theor. Biol. 121, 381–402.
Ge, Q.J., Inthavong, K., Tu, J.Y., 2012. Local deposition fractions of ultrafine particles in a human nasal-sinus cavity CFD model. Inhalation Toxicol. 24, 492–505.
Gelman, R.A., Meyer, F.A., 1979. Mucociliary transference rate and mucus viscoelasticity dependence on dynamic storage and loss modulus. Am. Rev. Respir. Dis. 120, 553–557.
Gizurarson, S., 2015. The effect of cilia and the mucociliary clearance on successful drug delivery. Biol. Pharm. Bull. 38, 497–506.
Halama, A.R., Decreton, S., Bijloos, J.M., Clement, P.A., 1990. Density of epithelial cells in the normal human nose and the paranasal sinus mucosa. A scanning electron microscopic study. Rhinology 28, 25–32.
Illum, L., 2003. Nasal drug delivery—possibilities, problems and solutions. J. Control. Release 87, 187–198.
Inthavong, K., Shang, Y.D., Tu, J.Y., 2014. Surface mapping for visualization of wall stresses during inhalation in a human nasal cavity. Resp. Physiol. Neurobiol. 190, 54–61.
King, M., Agarwal, M., Shukla, J., 1993. A planar model for mucociliary transport: effect of mucus viscoelasticity. Biorheology 30, 49–61.
Lale, A., Mason, J., Jones, N., 1998. Mucociliary transport and its assessment: a review. Clin. Otolaryngol. 23, 388–396.
Marttin, E., Schipper, N.G.M., Verhoef, J.C., Merkus, F.W.H.M., 1998. Nasal mucociliary clearance as a factor in nasal drug delivery. Adv. Drug Deliv. Rev. 29, 13–38.
Matsui, H., Randell, S.H., Peretti, S.W., Davis, C.W., Boucher, R.C., 1998. Coordinated clearance of periciliary liquid and mucus from airway surfaces. J. Clin. Investig. 102, 1125–1131.
Mestecky, J., Bienenstock, J., McGhee, J., Lamm, M.E., Strober, W., Cebra, J.J., Mayer, L., Ogra, P.L., 2005. Historical aspects of mucosal immunology. Mucosal Immunol., 23–43
Mistry, A., Stolnik, S., Illum, L., 2009. Nanoparticles for direct nose-to-brain delivery of drugs. Int. J. Pharm. 379, 146–157.
Mygind, N., Dahl, R., 1998. Anatomy, physiology and function of the nasal cavities in health and disease. Adv. Drug Deliv. Rev. 29, 3–12.
Pires, A., Fortuna, A., Alves, G., Falcão, A., 2009. Intranasal drug delivery: how, why and what for? J. Pharm. Pharmaceut. Sci. 12, 288–311.
Plaza Valia, P., Carrion Valero, F., Marin Pardo, J., Bautista Rentero, D., Gonzalez Monte, C., 2008. Saccharin test for the study of mucociliary clearance: reference values for a Spanish population. Archivos de bronconeumologia 44, 540–545.
Puchelle, E., Zahm, J., Quemada, D., 1987. Rheological properties controlling mucociliary frequency and respiratory mucus transport. Biorheology 24, 557–563.
Quinlan, M.F., Salman, S.D., Swift, D.L., Wagner Jr, H.N., Proctor, D.F., 1969. Measurement of mucociliary function in man. Am. Rev. Respiratory Dis. 99, 13–23.
Quraishi, M.S., Jones, N.S., Mason, J., 1998. The rheology of nasal mucus: a review. Clin. Otolaryngol. 23, 403–413.
Rusznak, C., Devalia, J., Lozewicz, S., Davies, R., 1994. The assessment of nasal mucociliary clearance and the effect of drugs. Respir. Med. 88, 89–101.
Rygg, A., Hindle, M., Longest, P.W., 2016. Absorption and clearance of pharmaceutical aerosols in the human nose: effects of nasal spray suspension particle size and properties. Pharm. Res. 33, 909–921.
Rygg, A., Longest, P.W., 2016. Absorption and clearance of pharmaceutical aerosols in the human nose: development of a CFD model. J. Aerosol Med. Pulmonary Drug Delivery 29, 416–431.
Satir, P., Sleigh, M.A., 1990. The physiology of cilia and mucociliary interactions. Annu. Rev. Physiol. 52, 137–155.
Schipper, N.G.M., Verhoef, J.C., Merkus, F.W.H.M., 1991. The nasal mucociliary clearance: relevance to nasal drug delivery. Pharm. Res. 8, 807–814.
Shah, S.A., Dickens, C.J., Ward, D.J., Banaszek, A.A., George, C., Horodnik, W., 2014. Design of experiments to optimize an in vitro cast to predict human nasal drug deposition. J. Aerosol Med. Pulmonary Drug Delivery 27, 21–29.
Shang, Y., Dong, J.L., Inthavong, K., Tu, J.Y., 2017. Computational fluid dynamics analysis of wall shear stresses between human and rat nasal cavities. Eur. J. Mech. B-Fluid. 61, 160–169.
Shang, Y., Tian, L., Fan, Y., Dong, J., Inthavong, K., Tu, J., 2018. Effect of morphology on nanoparticle transport and deposition in human upper tracheobronchial airways. J. Comput. Multiph. Flows. 1757482X18756012.
Shang, Y.D., Dong, J.L., Inthavong, K., Tu, J.Y., 2015. Comparative numerical modeling of inhaled micron-sized particle deposition in human and rat nasal cavities. Inhalation Toxicol. 27, 694–705.
Sleigh, M., 1977. The nature and action of respiratory tract cilia. Respiratory Defense Mechanisms. Part 1, 247–288.
Tong, X.W., Dong, J.L., Shang, Y.D., Inthavong, K., Tu, J.Y., 2016. Effects of nasal drug delivery device and its orientation on sprayed particle deposition in a realistic human nasal cavity. Comput. Biol. Med. 77, 40–48.
Ugwoke, M.I., Agu, R.U., Verbeke, N., Kinget, R., 2005. Nasal mucoadhesive drug delivery: background, applications, trends and future perspectives. Adv. Drug Deliv. Rev. 57, 1640–1665.
Verdugo, P., 1990. Goblet cells secretion and mucogenesis. Annu. Rev. Physiol. 52, 157–176.
Yergin, B.M., Saketkhoo, K., Michaelson, E.D., Serafini, S.M., Kovitz, K., Sackner, M.A., 1978. A roentgenographic method for measuring nasal mucous velocity. J. Appl. Physiol. 44, 964–968.